


Experimental Heat Transfer Coefficients for Zeotropic Mixture Condensation of Hexamethyldisiloxane/Octamethyltrisiloxane and Ethanol/Hexamethyldisiloxane

Conrad Zimmermann*, Nico Lubos, and Stephan Kabelac

DOI: 10.1002/cite.202300121

 This is an open access article under the terms of the Creative Commons Attribution-NonCommercial-NoDerivs License, which permits use and distribution in any medium, provided the original work is properly cited, the use is non-commercial and no modifications or adaptations are made.

Legal requirements for refrigerants necessitate a continuous development of these fluids, also focusing on mixtures. This article contributes three aspects to the ongoing research: (1) Experimental mean heat transfer coefficients were determined for the condensation of two novel zeotropic mixtures, hexamethyldisiloxane (MM)/octamethyltrisiloxane and ethanol/MM, gathered for filmwise condensation on a vertical tube. (2) Both mixtures were investigated with several compositions to provide a comprehensive understanding of the mixture effects. (3) The results were taken to develop a novel superposition approach to predict mixture condensation.

Keywords: Condensation, Heat transfer, Laminar film, Mixture, Siloxane

Received: August 03, 2023; *revised:* September 24, 2023; *accepted:* December 21, 2023

1 Introduction

Condensation heat transfer is omnipresent in process engineering, and many applications in the chemical industry deal with mixture condensation in particular. Furthermore, heat pumps, not only for small-scale space heating but also for high-temperature applications, undergo a strong increase due to the goal of decarbonization on a global scale. While these heat pumps rely on eco-friendly and energy-efficient working fluids, the number of suitable pure working fluids for heat pumps, refrigeration, and organic Rankine cycles (ORC) is very limited, as the working fluids face strict regulations concerning the global warming potential (GWP) or environmental sustainability [1]. One possibility to overcome this bottleneck is to establish mixtures with tailored properties [2]. However, the phase change behavior of zeotropic mixtures is more complex in comparison to that of pure fluids. The condensation of a zeotropic mixture is largely influenced by the vapor-liquid equilibrium (VLE), which leads to a continuous change of the compositions of the vapor and condensate phases and of the dew temperature over the whole process [3]. Although this so-called temperature glide may reduce the heat transfer coefficients (HTC), the non-isothermal phase change can also contribute to an improvement of the cycle performance, when the rising temperature of the heat sink aligns with the condensation curve of the mixture, consequently reducing the exergy loss during heat transfer [4]. Over the last years, various azeotropic and near-azeotropic mixtures of hydrofluor-

ocarbons (HFC) and hydrofluoroolefins (HFO) with small temperature glides were established to mitigate some of the negative ecological impacts of conventional pure fluids. In this context, Jacob and Fronk [5] investigated the condensation of a set of these commercially available mixtures with small temperature glides. Yet, a larger step towards zeotropic mixtures has not followed, so far, despite the possible benefits in the cycle efficiencies. This can be attributed, in part, to the lack of practical prediction methods for zeotropic mixture condensation, which hinders the quick evaluation of cycle performances of novel mixtures. Fronk and Garimella [3] give a summary of common calculation methods of mixture condensation HTC. These are still cumbersome and need extensive thermophysical mixture properties, which are often unavailable for novel mixtures. Furthermore, the physical explanations for the deterioration of heat transfer coefficients during mixture condensation in comparison to pure fluid condensation differ. The non-equilibrium approach by Colburn and Drew [6] highlights the mass transfer resistance in the interface boundary layer, while the equilibrium approach by Silver [7] and Bell and Ghaly [8], in turn, emphasizes the condensation path and

¹Conrad Zimmermann  <https://orcid.org/0000-0002-3161-0974> (zimmermann@ift.uni-hannover.de), ¹Nico Lubos,

¹Prof. Dr.-Ing. Stephan Kabelac

¹Institute of Thermodynamics, Leibniz University Hannover, Welfengarten 1, 30167 Hannover, Germany.

solely heat transfer resistances according to Webb et al. [9]. On the contrary, another study by Dorao and Fernandino [10] states that the differences in thermophysical properties are the main reason for the heat transfer deterioration, while others [11] observe the temperature glide as most influential.

Although the number of experimental studies on condensation heat transfer of mixtures increased in the last years, a substantial characterization of the most influential mixture effects over a wide composition range is still needed, in order not to get lost in the overabundance of potential refrigerant mixtures. It is the systematic experiments as conducted by Zhang et al. [11] or Mazumder et al. [12] that contribute to further development of practical prediction methods for the heat transfer coefficients of mixture condensation. Therefore, the present article provides experimental data of film condensation on a vertical tube for two binary mixtures, hexamethyldisiloxane/octamethyltrisiloxane (MM/MDM) and ethanol/MM, in a wide range of compositions. It is a follow-up to the experimental data on mixture condensation of ethanol/water and ethanol/MDM published by Zimmermann et al. [13]. The new results support a comprehensive discussion of the most influential mixture effects during condensation and extend the development of a superposition (SP) approach for the practical prediction of mean heat transfer coefficients.

2 Methods

2.1 Experimental Setup and Investigated Mixtures

The experimental setup is a closed loop with a pool boiler, which provides mixture vapor for the condenser section. A description of the entire test rig can be found in [13], and thus, the present publication only recapitulates the main aspects of the system. The condenser section, which is essential for the measurement of the heat transfer coefficients, is presented in a detailed schematic overview with the relevant instrumentation in Fig. 1. All temperature sensors are calibrated prior to the measurements with a Pt25 reference thermometer. The resulting uncertainties of the measuring devices are also given in [13]. The vapor inlet and outlet temperatures are measured with thermocouples of type K, placed in the center of the pipes. Sufficient mixing of the vapor flow is assumed to be achieved by the turbulence promoted by pipe bending and high vapor Reynolds numbers. However, both vapor temperatures have a minor influence on the calculation of the resulting HTC, while the saturation pressure at the inlet and the temperature difference of the thermostat

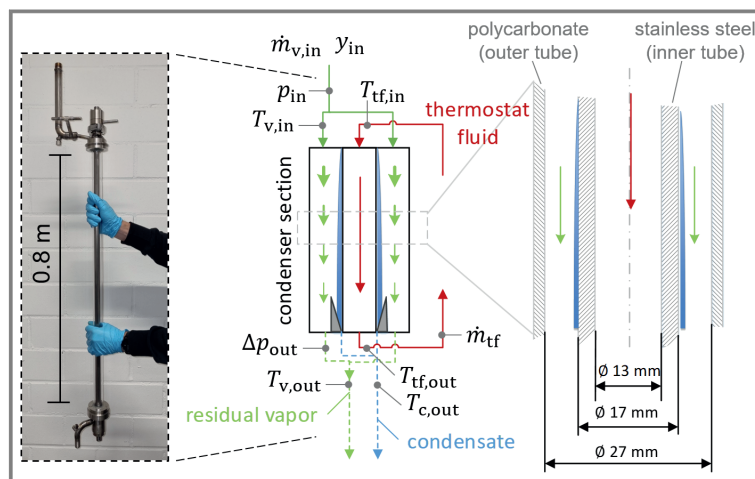


Figure 1. Condenser section with geometry and instrumentation.

fluid are most influential, but these quantities have higher accuracies and are less sensitive to flow conditions.

The experiments comprise mixture condensation of MM/MDM and ethanol/MM with various compositions, as well as the pure fluid condensation of the given substances. A summary of the most relevant thermophysical properties of the pure fluids is shown in Tab. 1. These are obtained from the CHEMCAD [14] library and also taken for the evaluation of the HTC in Sect. 2.2. Furthermore, the VLE of both mixtures are presented in Fig. 2 and again calculated with CHEMCAD using the UNIFAC [15] model. The lower pressure of 0.25 bar in Fig. 2 corresponds to the typical mean operating pressure of the experiments.

Fig. 2 reveals that the shapes of the VLE are distinctly different: The VLE of MM/MDM is mostly symmetric with a maximum temperature glide T_{glide} of about 18 K at around 50 wt % MM, while ethanol/MM has an azeotropic point at a mass fraction of $y_{\text{eth}} = 0.32 \dots 0.4$, depending on the pressure. This article, however, investigates only mass fractions of ethanol smaller than the azeotropic composition, where the maximum temperature glide is about 13 K at an ethanol mass fraction of about 5 wt %. In comparison to the mixture of ethanol/MDM, which was investigated in the previous publication [13] with a larger temperature glide of up to

Table 1. Thermophysical properties of the pure fluids.

Property at 20 °C and 1 bar	MDM (> 97.0 % purity)	MM (> 98.0 % purity)	Ethanol (> 99.8 % purity)
λ_1 [W m ⁻¹ K ⁻¹]	0.132	0.105	0.164
$\eta_1 \times 10^{-3}$ [kg m ⁻¹ s ⁻¹]	0.887	0.510	1.194
ρ_1 [kg m ⁻³]	820	765	789
$h_{v,1}$ (1 bar) $\times 10^3$ [J kg ⁻¹]	153	225	850
$c_{p,1}$ [J kg ⁻¹ K ⁻¹]	1483	1905	2396
$\sigma_1 \times 10^{-3}$ [N m ⁻¹]	17.1	15.8	22.5

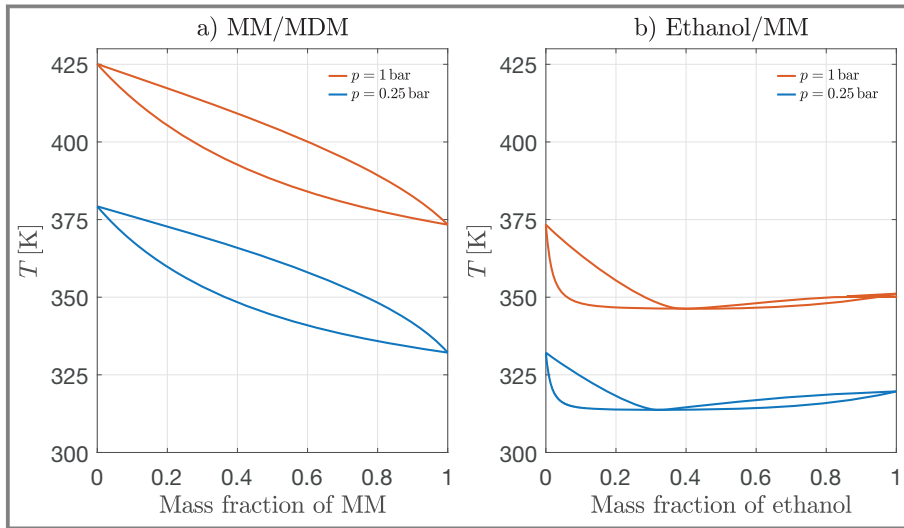


Figure 2. VLE of MM/MDM and ethanol/MM.

42 K at 9 wt % of ethanol, the two novel mixtures consequently extend the variety of VLE shapes in order to gain a comprehensive understanding of the influence on mixture condensation heat transfer.

2.2 Evaluation of HTC

In general, calculation of the mean HTC, α_{con} , of the mixture condensation experiments is deduced from the overall heat transmission in Eq. (1) between the vapor and the cooling fluid.

$$\frac{1}{\alpha_{\text{con}} A_o} = \frac{\Delta T_{\text{log}}}{\dot{Q}_{\text{con}}} - \frac{1}{\alpha_i A_i} - \frac{1}{2\lambda_{\text{st}} \pi L} \ln\left(\frac{A_o}{A_i}\right) \quad (1)$$

Here, α_i is the HTC between the thermostat fluid and the inner wall of the stainless-steel pipe, calculated with a correlation of Gnielinski [16]. The pipe has the length L , with an inner surface area A_i , an outer surface area A_o , and the thermal conductivity $\lambda_{\text{st}} = 15 \text{ W m}^{-1} \text{ K}^{-1}$. The heat flow \dot{Q}_{con} associated with the condensation is calculated by means of an energy balance for the thermostat fluid (water) minus sensible cooling of the vapor.

$$\dot{Q}_{\text{con}} = \dot{m}_{\text{tf}} \bar{c}_{\text{tf}} (T_{\text{tf,out}} - T_{\text{tf,in}}) - \dot{m}_{\text{v,in}} \bar{c}_{\text{p,v}} (T_{\text{v,in}} - T_{\text{d,in}}) \quad (2)$$

The dew temperature $T_{\text{d,in}}$ of the vapor is derived from the pressure and composition at the inlet. The vapor is only slightly superheated when entering the test section, to prevent prior condensation; yet, film condensation can be observed from the very top of the pipe. Therefore, the whole condenser length is taken as the effective heat transfer area and the desuperheating is considered to be negligible. The positioning of all necessary temperature measurements in Eq. (2) can be taken from Fig. 1. These temperatures are also

employed for the calculation of the logarithmic mean temperature difference (LMTD), ΔT_{log} .

$$\Delta T_{\text{log}} = \frac{(T_{\text{d,in}} - T_{\text{tf,in}}) - (T_{\text{v,out}} - T_{\text{tf,out}})}{\ln\left(\frac{T_{\text{d,in}} - T_{\text{tf,in}}}{T_{\text{v,out}} - T_{\text{tf,out}}}\right)} \quad (3)$$

Necessary thermophysical data are evaluated from the pressure measurement with an arithmetic mean pressure p_m between the inlet and the outlet. This is sufficiently accurate due to low pressure differences in all operating points of less than 5 mbar. Tab. 2 lists the mean relative combined standard uncertainties of all different compositions for the operating

points with total condensation. In the following figures, the uncertainty bars are omitted for reasons of improved readability. In general, the temperature difference between the inlet and outlet of the thermostat fluid has the largest impact on the uncertainty. Therefore, this difference should be significantly larger than the uncertainty of the temperature measurement and it can be adjusted by decreasing the mass flow rate of the thermostat fluid. However, a smaller mass flow rate reduces the HTC of the thermostat fluid α_i , which should be kept between 2000 and $3500 \text{ W m}^{-2} \text{ K}^{-1}$ in order to maintain a minor thermal resistance in Eq. (1). Finally, this leads to a lower combined standard uncertainty of α_{con} . Further information on the measurement uncertainties and experimental procedure are given in the previous publication [13].

Table 2. Mean relative combined standard uncertainties for operating points with total condensation.

Mixture of MM/MDM	
Mass fraction of MM [%]	$u_m(\alpha_{\text{con,tc}})$ [%]
26	21.5
54	14.2
91	14.8
Mixture of ethanol/MM	
Mass fraction of ethanol [%]	$u_m(\alpha_{\text{con,tc}})$ [%]
4.5	12.7
10	11.9
21.5	12.3
30.5	12.1

3 Experimental Results and Discussion

3.1 Pure Fluids

At first, the experimental results for the pure fluid condensation will be discussed, as these are taken to validate the setup and calculation procedure. Besides, the pure fluid condensation serves as a reference when compared with the mixture condensation. Consequently, Fig. 3 shows the mean HTC depending on the LMTD for the condensation of ethanol and MDM, which are recapitulations from [13], and the results for MM, which are new. The filled markers indicate that complete liquefaction is reached in the respective measuring points. Additionally, calculations of Nusselt's theory of laminar film condensation with a correction term for waviness by Kutateladze and Gogonin [17] are plotted in the same diagram. These correlations are well established and show good agreement with the experimental data. In general, the results in Fig. 3 show the typical functional behavior of filmwise condensation. The decreasing HTC for higher LMTD are caused by the increasing condensate film thickness, which represents a heat transfer resistance. The filmwise condensation can also be observed visually in all experiments. The larger deviation between the Nusselt calculation for MDM and the experimental results may be attributed to the lower purity of the substance of only 97 % (see Tab. 1), but overall, the mean relative deviation is typical of two-phase HTC.

3.2 MM/MDM

The study of the mixture condensation of MM/MDM is conducted with three different mass fractions of MM, which are chosen to cover a wide range of compositions. All mass fractions given in this section relate to the vapor at the condenser inlet and they always address the amount of the light component, MM. Fig. 4 shows the experimental results for the mixture condensation HTC of MM/MDM depending on the LMTD in combination with the same pure fluid results from Fig. 3. In this case, none of trend lines has any physical background but shall underline the connectivity of the particular series of data. It can be seen that the different mass flow rates for each of the investigated mass fractions mainly align in the overall qualitative trend of the particular composition. Thus, the mass flow rate does not significantly affect the HTC. This is in accordance with the theory of filmwise condensation, which can be observed visually for all cases of mixture condensation. With regard to the influence of different mass fractions of MM, it can be seen that

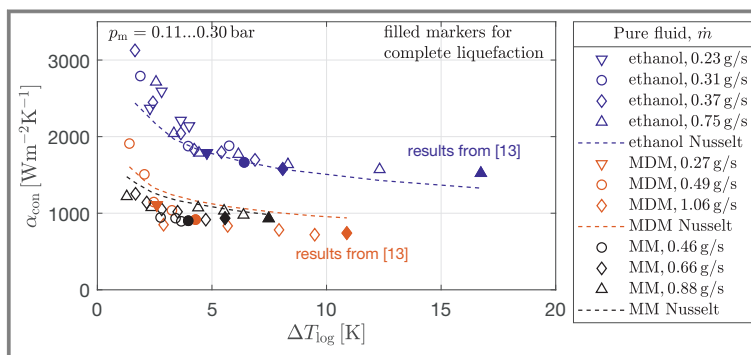


Figure 3. Mean HTC for pure fluid condensation of ethanol and MDM from [13], and new experimental results for MM compared with calculations of Nusselt's laminar film condensation.

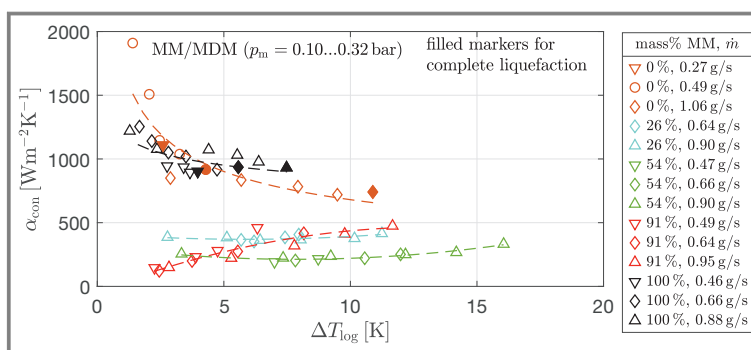


Figure 4. Mixture condensation HTC of MM/MDM with trend lines.

the mean HTC for 26 wt % of MM are distinctly smaller in comparison to those of pure MDM. However, the mean HTC are nearly constant and more or less independent of the LMTD, although different LMTD values lead to different vapor qualities and, hence, different mass fractions of the condensate at the outlet. The deterioration of the mean HTC intensifies for 54 wt % of MM, as expected. However, for larger LMTD values the HTC slightly increase. With 91 wt % MM, the HTC are generally lower than the values for pure MM as well, but the qualitative shape of the curve changes to the extent that the effect of the increasing HTC is dominant.

The different functional behaviors of the HTC depending on the mass fractions result from several mixture effects, which shall be evaluated in the following. Three main aspects are discussed in the light of the experimental results: (i) the influence of the VLE with the corresponding temperature glide, (ii) the influence of the different thermal properties of the condensate due to the continuous change of the composition, and (iii) the impact of the so-called condensation curve in combination with the potential heat of condensation of the mixture, which will be explained later on.

It is well known that the temperature glide has a strong impact on the deterioration of the mean HTC compared to pure fluids. While a pure fluid can be liquefied with just a

small subcooling of the wall below the saturation temperature of the vapor, the condensation of a mixture vapor terminates early for the same subcooling as the saturation temperature decreases continuously. Therefore, the same condensation rate can only be achieved with larger wall subcoolings, i.e. larger LMTD values, consequently resulting in smaller HTC. (i) Therefore, the HTC for 26 wt % of MM are smaller than those of the pure fluids due to a temperature glide of 15.2 K of the mixture. The HTC of 54 wt % MM are also decreased and slightly smaller than the HTC at 26 wt %, as a result of a minor increase of the temperature glide to 17.8 K. With regard to 91 wt % of MM, the HTC increase with larger LMTD values, and they are finally higher than for the other compositions, which corresponds to the smaller temperature glide of 7.4 K.

For all compositions of the MM/MDM mixture, aspect (ii) concerning the influence of different thermal properties can be mostly neglected, assuming that these mixture properties follow a typical steady trend between the pure fluid properties presented in Tab.1. The data reveals that the thermal properties of MM and MDM differ only slightly. This can also be found in the investigation of the pure fluid condensation in Fig. 3, where both pure fluids have almost identical HTC. However, the different functional behaviors of the mixture HTC in Fig. 4 need to be explained with the condensation curve and potential heat of condensation in Fig. 5.

Aspect (iii), the so-called condensation curve, is discussed based on Fig. 5a, which shows the progress of the dew temperature for the investigated inlet mass fractions over the vapor quality X . The data are taken from VLE calculations and do not refer to any experiments. A strong decline in the condensation curve represents a section of the condensation process where most of the sensible heat of the mixture is extracted. In this mixture, none of the curves shows significant slopes; thus, the sensible cooling occurs uniformly for all compositions. In addition, Fig. 5b provides the calculated latent heat that can potentially be extracted from the mixture vapor, depending on the temperature difference be-

tween the dew temperature of the mixture composition and the wall temperature T_w . It is referred to as a “potential” heat because an infinite surface area needs to be assumed to extract all the latent heat of condensation. The latent heat in this case is calculated by means of ideal mixing of the pure fluids, while the inferior amount of sensible heat from the temperature glide is neglected. As Fig. 5 only serves to provide additional explanations and not for further calculations, these simplifications seem justifiable. In the case of 91 wt % of MM, the potential heat of condensation increases exponentially with an increase of the wall subcooling. This corresponds to the HTC of 91 wt % of MM in Fig. 4, which increase for increasing LMTD as more latent heat can be extracted, while the temperature difference grows. The opposite behavior appears for 26 wt %, where an increase of the LMTD values in Fig. 4 does not affect the mean HTC. This is supported by Fig. 5, as the potential heat of condensation has a concave downwards shape.

3.3 Ethanol/MM

In analogy to MM/MDM, the experimental HTC of ethanol/MM depending on the LMTD are presented in Fig. 6 for different inlet mass fractions of ethanol smaller than the azeotropic composition. The results for 30.5 wt % are near-azeotropic. Starting with a mass fraction of 4.5 wt % of ethanol, the HTC are significantly lower than those of pure MM. This tendency persists for 10 wt %, although the qualitative behavior changes to a linear trend for increasing LMTD values. With 21.5 wt % of ethanol, the HTC start to significantly increase again until, with 30.5 wt %, the HTC almost exceed those of pure MM. Again, none of the compositions show a significant dependence on the mass flow rate, which verifies filmwise condensation, just as the visual observation does.

In general, the deterioration of the HTC is related to aspect (i), the temperature glide, which is maximum 12.7 K for 4.5 wt % and 10.7 K for 10 wt % of ethanol. Yet, the temperature glide for 21.5 wt % ethanol is much smaller with 4.1 K, but still leads to significantly lower HTC than in case of the pure fluid. On top of that, the increased amount of ethanol should already induce an improved performance on behalf of the thermophysical properties of ethanol, which are superior to those of MM. In contrast to the mixture of MM/MDM, where both components have very similar properties, the combination of ethanol/MM needs consideration of aspect (ii) with the different compositions and thermal properties especially in the liquid condensate phase. The VLE in Fig. 2 reveals that the heavy component MM condenses predomi-

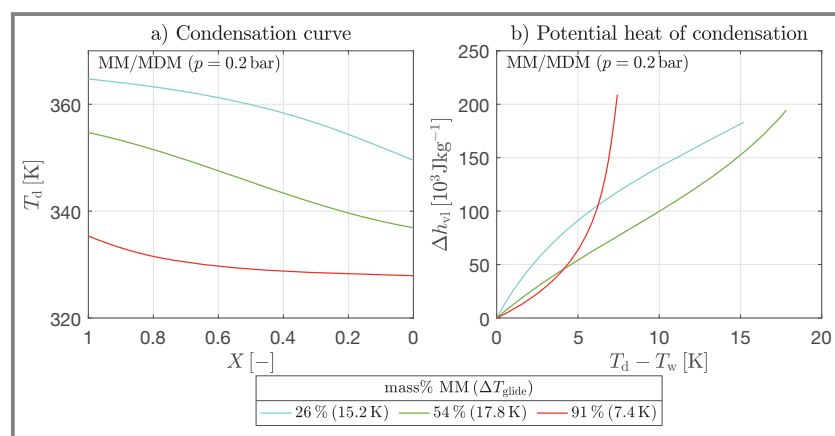


Figure 5. Condensation curve and potential heat of condensation for MM/MDM.

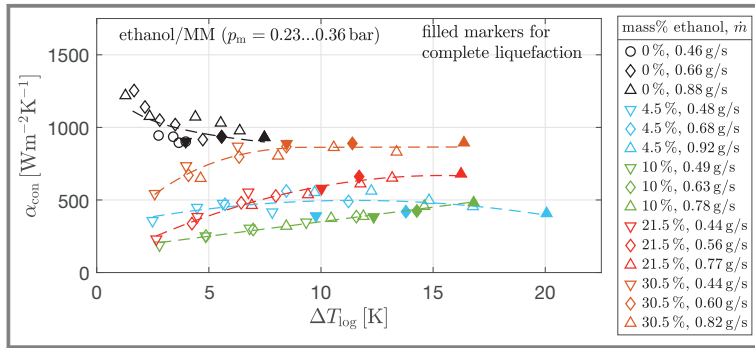


Figure 6. Mixture condensation HTC of ethanol/MM with trend lines.

nantly and ultimately rules the heat transfer through the condensate layer over the whole process. As a consequence, the HTC are decreased not only by the temperature glide but also by the thermophysical properties of MM.

Moreover, the data of ethanol mass fractions of 10%, 21.5% and 30.5% in Fig. 6 show increasing HTC for higher LMTD values. Once more, (iii) the potential heat of condensation is responsible for these trends, as the compositions show an exponential growth in Fig. 7b with larger temperature differences. In principle, the curvature of the condensation curve is reflected in the shape of the potential heat of condensation, but it also contributes to further explanation of the observed behavior. For example, the HTC of the mixture with 4.5 wt% ethanol in Fig. 6 decrease slightly with larger LMTD values. Looking at a residual vapor quality of 0.2 in Fig. 7a, it can be seen that the mixture of 4.5 wt% still needs to extract approximately 5 K of sensible heat to reach complete liquefaction. In comparison, the mixture with 10 wt% has about 1 K of sensible heat left. Now, the condensate layer in both cases should have a similar thickness, as the residual vapor quality is the same. However, the condensate layer hinders the sensible cooling, which is crucial if a larger part of the sensible cooling still needs to be fulfilled. Hence, larger wall subcoolings are nec-

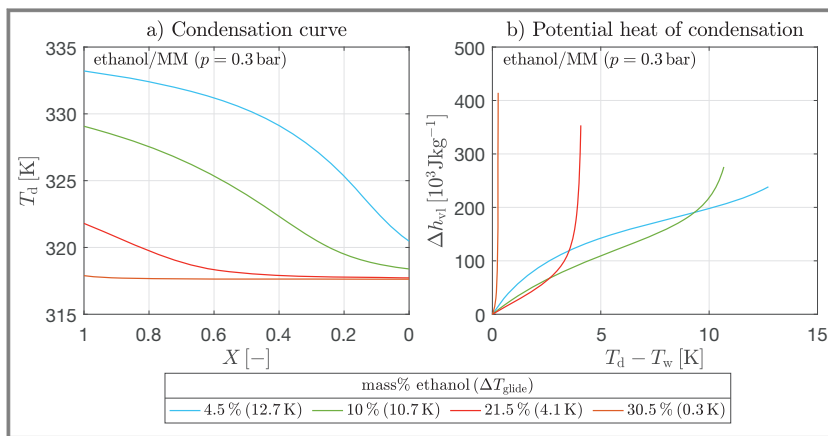


Figure 7. Condensation curve and potential heat of condensation for ethanol/MM.

essary to achieve complete liquefaction and this reduces the HTC of 4.5 wt% ethanol. The opposite appears for 21.5 wt%, where most of the sensible cooling happens at the beginning of the condenser with a thin condensate layer and, later in the process, only latent heat needs to be extracted.

4 Conclusion and Outlook

The previous results and explanations outline major influential aspects that affect the HTC of mixture condensation. With regard to the findings from Zhang et al. [11], the temperature glide can be affirmed as the major effect that governs the deterioration of the mean HTC. Additionally, composition-dependent mixture properties do not have the strongest influence on HTC, but they become relevant in a precise evaluation of the HTC. Probably, this influence of mixture properties increases for mixtures with small temperature glides. The present article also underlines that the condensation curve and the potential heat of condensation, as part of the mixture properties related to the VLE, should be taken into detailed consideration of mixture effects as well. Apart from that, mass transfer resistances, which are implemented in some calculation approaches in the literature, seem to be less influential. This discussion underlines that the complex interactions of different mixture effects need further investigation and sophisticated data engineering to elaborate a universal but practical prediction method for mean HTC.

In the earlier publication by Zimmermann et al. [13], a superposition (SP) approach for the fast approximate calculation of mixture condensation HTC based on pure fluid HTC is introduced. This approach is given by the following equation:

$$\alpha_{\text{con}} = y \cdot \alpha_{\text{con,LC,0}} \cdot \exp(-a_{\text{LC}}(1-y)^{b_{\text{LC}}}) + (1-y) \cdot \alpha_{\text{con,HC,0}} \cdot \exp(-a_{\text{HC}} \cdot y^{b_{\text{HC}}}) \quad (4)$$

The pure fluid HTC of the heavy component (HC) and light component (LC) are weighted by means of the vapor mass fraction at the inlet with an exponential correction term including dimensionless adjustable parameters, a_{LC} , a_{HC} , b_{LC} , and b_{HC} . These parameters are specific to the mixture and allow for the discussed mixture effects. Fig. 8 shows calculated mean HTC of the SP approach depending on the mass fraction of the LC at the inlet. The pure fluid HTC, as part of Eq. (4), are again calculated with Nusselt's

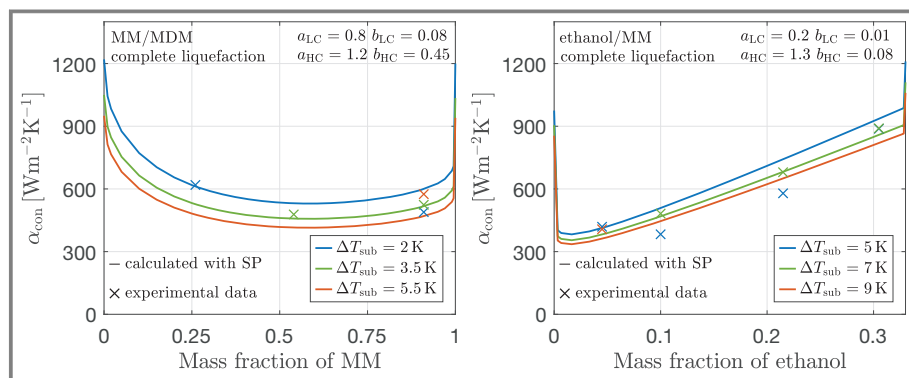


Figure 8. Comparison of experimental results with the SP approach.

correlation for laminar film condensation and a waviness correction factor by [17], just as in the validation in Sect. 3.1. The parameters of the SP approach are fitted to the given operating points with complete liquefaction.

The experimental and calculated results show good agreement although certain aspects need further development in future works: The edge region of the calculations with small mass fractions of the LC or HC show very large gradients, which seem physically inaccurate. This results from the functional behavior of the parameter $b_{LC/HC}$ and is partly necessary to achieve small deviations with the experimental data in other parts of the composition range. Still, this extreme behavior aligns with reported phenomena, which estimate a strong decline of the HTC as soon as a pure fluid undergoes even small impurities. Besides, the experimental data shows a dependency on the wall subcooling that is not covered with the parameters, yet. However, the fitted parameters and the SP approach already provide a practical correlation for quick calculation of mean HTC.

In the future, the fitted individual mixture parameters shall be expressed as generalized correlations based on dimensionless numbers that take the discussed mixture effects into account. For this reason, a detailed discussion of mixture effects as in Sects. 3.2 and 3.3 for several fluid combinations with different VLE and varying operating conditions is necessary to develop a comprehensive and thermodynamically valid description. The roles of the condensation curve and the potential heat of condensation have to be analyzed in more detail. Finally, the generalized SP approach could reduce costly validation experiments for the design of condensers with novel mixtures and provide a pre-design method based on readily accessible pure-fluid HTC.

Acknowledgment

The authors highly appreciate the funding of this project (no. 401366378) by the German Research Foundation (DFG). Open access funding enabled and organized by Projekt DEAL.

Symbols used

A	$[m^2]$	surface area
a, b	$[-]$	dimensionless parameters
\bar{c}_{tf}	$[J kg^{-1}K^{-1}]$	mean specific heat capacity of the thermostat fluid
$\bar{c}_{p,v}$	$[J kg^{-1}K^{-1}]$	mean isobaric specific heat capacity of superheated vapor
Δh_{vl}	$[J kg^{-1}]$	specific enthalpy of vaporization
L	$[m]$	length
\dot{m}	$[kg s^{-1}]$	mass flow rate
p	$[bar]$	pressure
\dot{Q}	$[W]$	heat flow rate
T	$[K]$	temperature
ΔT_{log}	$[K]$	logarithmic mean temperature difference
X	$[-]$	vapor quality, $\dot{m}_v/(\dot{m}_v + \dot{m}_l)$
y	$[kg kg^{-1}]$	mass fraction

Greek symbols

α	$[W m^{-2}K^{-1}]$	heat transfer coefficient
η	$[Pa s]$	dynamic viscosity
λ	$[W m^{-1}K^{-1}]$	thermal conductivity
ρ	$[kg m^{-3}]$	density
σ	$[N m^{-1}]$	surface tension

Sub-/superscripts

0	pure substance
b	bubble line
con	condensation
d	dew line
HC	heavy component
i	inner
in	inlet
l	liquid
LC	light component
m	mean
o	outer
out	outlet

s	saturated
st	stainless steel
sub	subcooled below the bubble line
tc	total condensation
tf	thermostat fluid
tot	total
v	vapor
w	wall

Abbreviations

HTC	heat transfer coefficient
LMTD	logarithmic mean temperature difference
MDM	octamethyltrisiloxane
MM	hexamethyldisiloxane
SP	superposition
VLE	vapor-liquid equilibrium

References

- [1] K. Harby, *Renewable Sustainable Energy Rev.* **2017**, *73*, 1247–1264. DOI: <https://doi.org/10.1016/j.rser.2017.02.039>
- [2] M. Kruzel, T. Bohdal, K. Dutkowski, W. Kuczyński, K. Chliszcz, *Energies* **2022**, *15* (6), 2241. DOI: <https://doi.org/10.3390/en15062241>
- [3] B. M. Fronk, S. Garimella, *Int. J. Refrig.* **2013**, *36*, 534–561.
- [4] T. Weith, F. Heberle, M. Preißinger, D. Brüggemann, *Energies* **2014**, *7* (9), 5548–5565. DOI: <https://doi.org/10.3390/en7095548>
- [5] T. A. Jacob, B. M. Fronk, *Int. J. Heat Mass Transfer* **2021**, *170*, 120947. DOI: <https://doi.org/10.1016/j.ijheatmasstransfer.2021.120947>
- [6] A. P. Colburn, T. B. Drew, *AIChE J.* **1937**, 197–212.
- [7] L. Silver, *Chem. Eng.* **1947**, 380–386.
- [8] K. J. Bell, M. A. Ghaly, *J. Heat Transfer* **1973**, *131* (69), 72–79.
- [9] D. R. Webb, M. Fahrner, R. Schwaab, *Int. J. Heat Mass Transfer* **1996**, *39* (15), 3147–3156.
- [10] C. A. Dorao, M. Ferdinando, *Appl. Phys. Lett.* **2019**, *114*, 171902. DOI: <https://doi.org/10.1063/1.5086738>
- [11] J. Zhang, B. Elmegaard, F. Haglind, *Int. J. Heat Mass Transfer* **2021**, *164*, 120577. DOI: <https://doi.org/10.1016/j.ijheatmasstransfer.2020.120577>
- [12] S. Mazumder, H. M. M. Afroz, M. A. Hossain, A. Miyara, S. Talukdar, *Int. J. Heat Mass Transfer* **2021**, *169*, 120859.
- [13] C. Zimmermann, N. Lubos, C. Dagli, S. Kabelac, *Chem. Ing. Tech.* **2023**, *95* (5), 724–731. DOI: <https://doi.org/10.1002/cite.202200198>
- [14] Chemstations Inc., CHEMCAD Version 8.0.0.14834, **2020**.
- [15] A. Fredenslund, R. L. Jones, J. M. Prausnitz, *AIChE J.* **1975**, *21* (6), 1086–1099. DOI: <https://doi.org/10.1002/aic.690210607>
- [16] V. Gnielinski, *AIChE J.* **1976**, *16* (2), 359–368.
- [17] S. S. Kutateladze, I. I. Gogonin, *Int. J. Heat Mass Transfer* **1979**, *22* (12), 1593–1599. DOI: [https://doi.org/10.1016/0017-9310\(79\)90075-9](https://doi.org/10.1016/0017-9310(79)90075-9)

DOI: 10.1002/cite.20230000121

Experimental Heat Transfer Coefficients for Zeotropic Mixture Condensation of Hexamethyldisiloxane/Octamethyltrisiloxane and Ethanol/Hexamethyldisiloxane

Conrad Zimmermann*, Nico Lubos, Stephan Kabelac

Research Article: Experimental data is presented for mixture condensation within a wide composition range. Different aspects in the heat transfer deterioration of mixtures are discussed. The results serve to develop a novel superposition approach for the approximate calculation of mixture condensation heat transfer coefficients. ■

